Research Article | Vol. 27, No. 20 / 30 September 2019 / Optics Express 28494

Optics EXPRESS

Speckle-based strain sensing in multimode fiber

MATTHEW J. MURRAY,* ALLEN DAVIS, CLAY KIRKENDALL, AND BRANDON REDDING

Optical Sciences Division, U.S. Naval Research Laboratory, 4555 Overlook Ave. SW, Washington, D.C. 20375, USA

matthew.murray@nrl.navy.mil

Abstract: The diversity of spatial modes present within a multimode fiber has been exploited for a wide variety of imaging and sensing applications. Here, we show that this diversity of modes can also be used to perform quantitative strain sensing by measuring the amplitude of the Rayleigh backscattered speckle pattern in a multimode fiber. While most Rayleigh based fiber sensors use single mode fiber, multimode fiber has the potential to provide lower noise due to the higher capture fraction of Rayleigh scattered light, higher non-linear thresholds, and the ability to avoid signal fading by measuring many spatial modes simultaneously. Moreover, while amplitude measuring single mode fiber based Rayleigh sensors cannot provide quantitative strain information, the backscattered speckle pattern formed in a multimode fiber contains enough information to extract a linear strain response. Here, we show that by tracking the evolution of the backscattered speckle pattern, the sensor provides a linear strain response and is immune to signal fading. The sensor has a noise floor of 2.9 $p\varepsilon/\sqrt{Hz}$, a dynamic range of 74 dB at 1 kHz, and bandwidth of 20 kHz. This work paves the way for a new class of fiber optic sensors with a simplified design and enhanced performance.

1. Introduction

Recent advances in high-speed imaging, wavefront shaping, and computational processing have sparked renewed interest in multimode fibers for applications as diverse as fiber optic communications [1,2], endoscopy [3], spectroscopy [4], and non-linear light generation [5]. These applications take advantage of the rich diversity of spatial, spectral and polarization modes to provide functionality and performance beyond what can be achieved using single mode fiber. In this work, we show that this diversity of spatial modes can also be used to realize a quantitative fiber optic strain sensor with localized response and state of the art performance.

Distributed fiber optic strain sensors are used for a wide range of applications including structural health monitoring [6,7], intrusion detection [8], and acoustic sensing [9]. Fiber strain sensors can be realized by introducing dedicated couplers to build Mach-Zehnder interferometers [10–12] or by writing fiber Bragg gratings (FBG) into the fiber [13]. In addition, Rayleigh based strain sensors such as those that use optical time domain reflectometry (OTDR) are particularly attractive since they enable highly distributed sensing using unmodified off-the-shelf fiber [14–17]. However, the vast majority of OTDR systems use single mode fiber (SMF), which imposes two significant limitations. First, OTDR systems are often light-limited due to the relatively weak Rayleigh backscattering [18] and the limits on the maximum input power imposed by non-linear effects such as stimulated Brillouin scattering and four-wave mixing. As a result, the noise performance of existing SMF OTDR systems is significantly worse than FBG based strain sensors which can provide much higher reflectivity. Second, SMF-based OTDR systems are susceptible to signal fading which occurs when the Rayleigh backscattered light interferes destructively with itself [19]. While the issue of signal fading can be substantially reduced in SMF systems using optical frequency multiplexing, the additional optical components required increases the system cost and complexity [20,21].

Multimode fibers have the potential to address both of these issues. First, multimode fiber offers the potential for increased backscattered light levels due to the higher capture fraction

#371247 https://doi.org/10.1364/OE.27.028494
Journal © 2019 Received 10 Jul 2019; revised 16 Aug 2019; accepted 8 Sep 2019; published 20 Sep 2019

Optics EXPRESS

of Rayleigh scattered light [18] and the ability to use higher input powers due to the higher non-linear thresholds in multimode fibers. Second, the issue of signal fading can be completely avoided. In a multimode fiber, the diversity of modes ensures that while the backscattered light may fade in any one mode, a large number of additional modes will be available to perform a measurement.

A handful of researchers have investigated strain sensing with multimode fiber using so-called fiber specklegram sensors [22–25]. In contrast to the backscattered light used in this work, fiber specklegram sensors operate by monitoring the light *transmitted* through a multimode fiber. While these sensors have shown a linear response to strain, their transmission mode design imposes several limitations: fiber speckegram sensors cannot provide a measurement of the local strain at specific positions along the fiber, cannot be extended to distributed sensing, and require access to both ends of the fiber. In addition, the transmitted speckle pattern is far less sensitive to strain than the Rayleigh backscattered pattern, typically limiting these sensors to $\mu\varepsilon$-level noise floors.

Recently, we demonstrated a multimode fiber (MMF) based phase-measuring Φ-OTDR system designed to take advantage of many of the features of sensing with multimode fiber by using a high-speed camera to record the entire backscattered speckle pattern [26]. This work confirmed that a linear strain response could be achieved in a multimode fiber and exhibited lower noise than most existing single mode fiber based OTDR systems. However, the system operated according to the same principle as SMF-based phase measuring OTDR systems without taking advantage of the additional information provided by the diversity of spatial modes in the MMF. That is, the sensor measured the relative phase between light backscattered from two distinct regions of the fiber, sometimes called "virtual mirrors". As such, this approach was designed to measure the strain in the region of fiber between these virtual mirrors and operates with an underlying assumption that there is no strain on the virtual mirror itself. Justifying this assumption drives the design to use shorter pulses resulting in smaller virtual mirrors and a reduced sensitivity to strain in the virtual mirror region at the cost of lower return light levels (assuming a fixed pulse peak power) and higher noise. The second limitation of this approach concerns the detection method. Phase measuring OTDR is typically achieved in one of two ways: (1) The phase of the backscattered light from the virtual mirrors can be measured with respect to an external reference arm and the relative phase between virtual mirrors can be extracted computationally. This was the approach taken in our previous MMF work [26] and the primary limitation is that this imposes significant constraints on the laser phase noise since a single reference arm can only be path-matched for one virtual mirror. In addition, common-mode rejection of signals outside the desired sensor position are limited by the signal-to-noise ratio of the measurement on each virtual mirror. (2) Alternatively, the relative phase between the backscattered light from two virtual mirrors can be measured directly by temporally aligning the two returns using a path-mismatched interferometer [16]. The trade-off in this case involves the inability to overcome the detector dark noise in the absence of a strong reference arm. This also limits the reconfigurability of the sensor, since a physical delay line is required to define the sensor size.

In this work, we introduce a new approach to quantitative strain sensing that is not possible in single mode fiber. The approach takes full advantage of the diversity of spatial modes present in multimode fiber to overcome the trade-offs in our previous work and the limitations inherent to specklegram sensors. Specifically, we show that by monitoring the temporal evolution of the amplitude of the backscattered speckle pattern from a single region of fiber we can extract the strain experienced by that region of fiber. Unlike single mode fiber based amplitude-measuring OTDR systems, the diversity of spatial modes provides sufficient information to extract a linear, quantitative measurement of the strain experienced in the fiber. In contrast to our prior work, the sensor region and the virtual mirror are now the same, enabling longer pulses and higher return light levels while avoiding the requirement that strain be confined to the region between

Optics EXPRESS

two virtual mirrors. Additionally, since the strain can be extracted directly from the amplitude of the speckle pattern, we are able to use a strong reference arm to overcome the dark noise on our camera without imposing severe laser phase noise requirements. This approach is inherently insensitive to strain outside the sensor region since the backscattered speckle pattern from a given region is, to first order, dictated only by the relative position of the scattering centers within the sensor region [19].

2. Operating principles

Rayleigh-based sensors operate by measuring the light scattered off small fluctuations in the fiber density and refractive index. In a multimode fiber, we can express the Rayleigh backscattered electric field by adapting the standard one-dimensional impulse response model [19]:

$$E(x,y,t) = \sum_{n=1}^{N}\sum_{m=1}^{M} r_n a_m \psi_m(x,y)\exp(i2\pi\nu t + i2\beta_m(z_n + dz_n(t)))\text{rect}\left(\frac{t-\tau}{T}\right) \tag{1}$$

where r_n is a measure of the reflectivity of the n^{th} scattering center, a_m is the amplitude of the m^{th} spatial mode, $\psi_m(x,y)$is the spatial profile of the m^{th} mode, β_m is the propagation constant of the m^{th} mode, z_n is the position of the n^{th} scatterer, and $dz_n(t)$ is the change in position of the n^{th} scatterer as a result of strain to the fiber. Assuming uniform axial strain across the sensor region, this change in position can be expressed as: $dz_n(t) = \xi\varepsilon z_n$, where ξ is the elasto-optic coefficient and ε is the axial strain. M is the total number of excited modes and N is the number of scattering centers. τ is the delay to the desired sensor region within the fiber and T is the pulsewidth of the incident light. Interference between the backscattered modes produces a seemingly random spatial pattern known as speckle. As strain is applied to the fiber, the speckle pattern fluctuates and this fluctuation carries information about the strain in the fiber. In this work, we show that it is possible to extract quantitative strain information from the fluctuations in the backscattered speckle pattern.

Our approach treats each speckle grain as if it is an independent interferometer at an arbitrary and unknown bias point. The individual speckle grains are formed by the summation of the electric field contributions of each spatial mode reflected from many scattering centers, each with a different phase delay. When the fiber experiences strain, the positions of the scattering centers will move changing these phase delays and thereby changing the amplitude of the speckle grains. The challenge is that this responsivity, or the change in amplitude for a given change in strain, is different for each speckle grain and is constantly changing. In addition, the sign of this responsivity factor can be different for each speckle grain and can change over time. Thus, at a given time, a positive strain will cause an increase in the amplitude of some speckle grains in the pattern while decreasing the amplitude of other speckle grains. Extracting a linear response requires us to first identify which speckle grains are increasing with strain and which speckle grains are decreasing with strain. To do this, we first make the assumption that changes in the speckle pattern are the result of a change in strain across the sensor (as opposed to shot noise in our measurement). Under this assumption, the change in amplitude of each speckle grain was induced by the same strain, thus providing a means to group speckle grains according to the sign of their responsivity. In other words, the speckle grains whose amplitude increased over some period of time have responsivity factors with a common sign, while speckle grains whose amplitudes decreased over this time range have responsivity factors with the opposite sign. After using this assumption to identify the "sign" of the responsivity for each speckle grain over time, we can then average the change in amplitude across the entire speckle pattern to achieve a linear strain response. One of the advantages of this approach is that the algorithm does not require any form of calibration since the strain is recovered from the evolution in the speckle pattern without requiring prior knowledge of the absolute speckle pattern produced at different levels of strain.

Optics EXPRESS

This approach also allows the fiber to be repositioned (e.g. bent or twisted) without requiring any form of re-calibration before continuing to use it as a sensor.

3. Speckle tracking processing and simulations

To develop and evaluate the speckle tracking algorithm, we first tested its performance on simulated data. The backscattered speckle pattern was simulated using the impulse response model given in Eq. (1) for linearly increasing strain. To reduce the computation time, we simulated a 1-dimensional multimode slab waveguide rather than a 2-dimensional fiber. The model ignores mode mixing and polarization effects. The spatial mode profiles and propagation constants were modeled according to [27] for 532 nm light propagating through a 50 μm wide multimode waveguide with a numerical aperture of 0.22 and an index of refraction of 1.46. The waveguide supported 42 modes and there were 100 scattering centers randomly distributed over a 10 m region located 10 m from the end of the simulated waveguide.

Figure 1(a) shows how the amplitude of the speckle pattern evolves with time on a grid of 2000 pixels with a spatial resolution of 25 nm. In Fig. 1(b), we highlight the evolution of three pixels, illustrating the non-linear change in amplitude under a linearly increasing strain. Note that a typical SMF based amplitude measuring OTDR sensor would measure a signal analogous to just one of these speckle grains over time. Without the additional information provided by monitoring many speckle grains in parallel, there would be no way to extract quantitative strain information from the evolution of any one of these speckle grains. Figure 1(c) highlights the periods when the pixel amplitude increases with increasing strain and periods when the amplitude decreases.

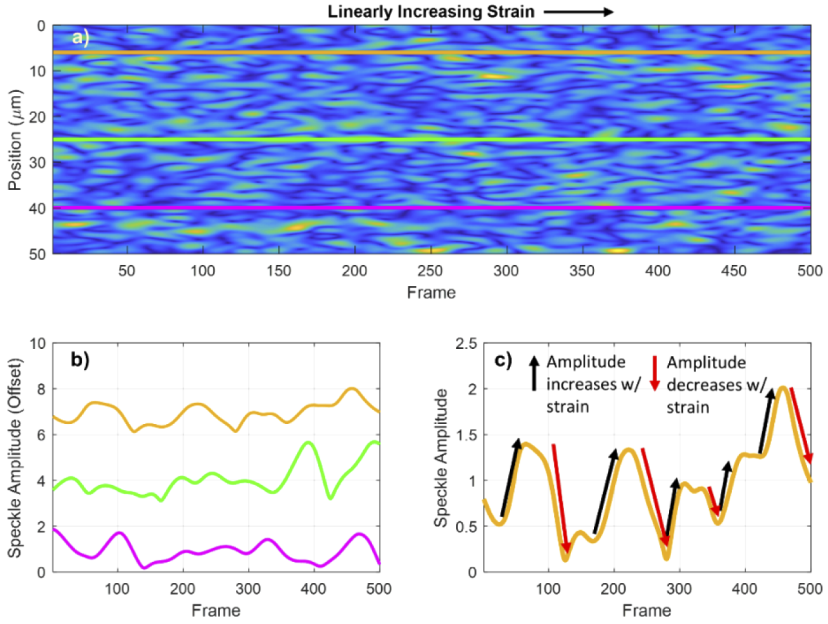

Fig. 1. a) The evolution of the speckle pattern on a grid of 2000 pixels as linear strain is applied to the fiber. b) The time evolution of the amplitude from three pixels. The data has been offset to show the evolution of each pixel. c) The evolution of one pixel with increasing strain. The speckle tracking algorithm identifies the regions when the pixel amplitude increases with strain and when the pixel amplitude decreases with strain.

We provide a detailed description of the algorithm in the Appendix. Here we give a brief overview of how we process the optical return image frames to extract the strain in the fiber. Each pixel is assigned a flag indicating whether its amplitude is trending positive or negative with

Optics EXPRESS

strain. This assignment is achieved by monitoring several frames of data and tracking the trend of each pixel amplitude. Successive frames are differenced to measure the change in amplitude of each pixel. The change in each pixel across the adjacent frames are then aligned in slope using their sign flags and summed across all pixels to determine the slope-corrected change in the returned optical amplitude. The slope-corrected change is then integrated across frames to recover the strain in the fiber. Since the slope of the amplitude for each pixel will eventually change with strain, we implement a test to determine when the sign flags need to be updated. Details regarding when the flags are updated can be found in the Appendix. In this work, the algorithm was implemented in post processing; however, the algorithm itself is entirely forward processing and thus the strain can be recovered in real time with some small latency.

The algorithm was first tested using the simulated data for linearly increasing strain. Figure 2(a) shows the amplitude of one pixel as a function of time along with the assigned pixel flags. In this case, since the strain was linearly increasing for the entire dataset, the pixel flags should simply match the sign of the slope of the speckle amplitude. It is clear from the figure that the algorithm correctly identifies when the amplitude increases with strain and when the amplitude decreases with strain. Figure 2(b) shows that the algorithm correctly recovers the linear strain.

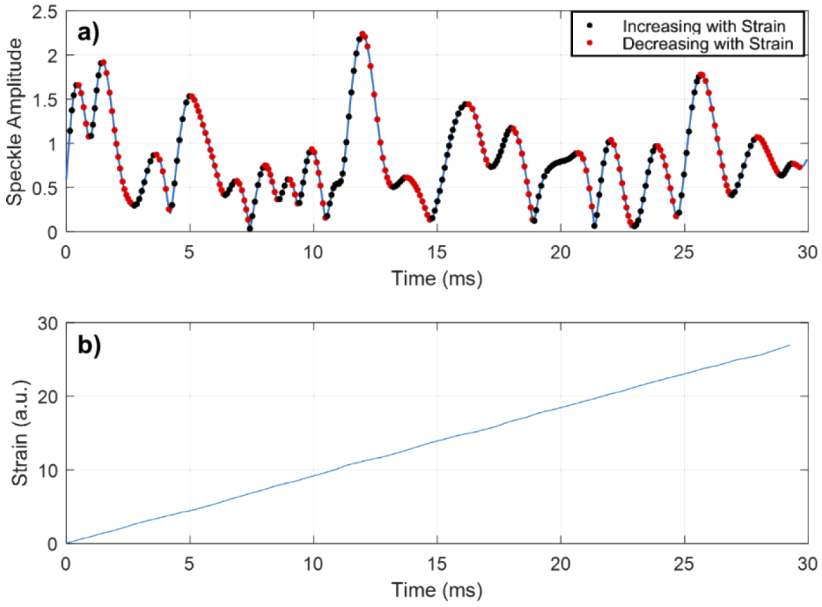

Fig. 2. a) Amplitude of a single pixel using the impulse response model to simulate the backscattered speckle evolution under a linearly increasing strain. The red and black dots indicate when the pixel flag has been updated. Black indicates that amplitude increases with increasing strain and red indicates that amplitude decreases with increasing strain. b) The recovered strain extracted from the amplitude fluctuations of the backscattered speckle pattern.

Note that the amplitude of the speckle pattern was normalized such that the average amplitude of the entire pattern was one. This converted the speckle pattern to a consistent normalized amplitude unit in both the simulated and experimental data. The sensor responsivity is then required to convert from normalized amplitude units (au) to units of strain. This responsivity is analogous to the conversion factor from radians to strain reported for traditional phase-measuring ϕ-OTDR systems [17,28]. The sensor responsivity in units of au/nε/m was first estimated by extracting the magnitude of the response to simulated data with known strain. In this case, the backscattered speckle pattern was simulated for a 20 nε sinusoidal strain at 1 kHz. We used the

Optics EXPRESS

same fiber parameters as in the linear strain simulation described earlier. The simulation was repeated 10 times at 7 different sensor lengths (pulsewidths) between 1 m and 20 m (10 ns and 200 ns, respectively). The average predicted sensor responsivity R is

$$R_{predict} = (4.51 \pm 0.16) \times 10^{-3} \text{au/n}\varepsilon\text{/m}$$

As expected, the responsivity did not show a dependence on the sensor length.

4. Experimental results

4.1. Sensor design and operation

In order to validate this approach experimentally, we first needed to record the time varying speckle pattern backscattered from a fiber under a known strain. To conduct this proof-of-principle demonstration, 532 nm light was used in order to leverage available high speed camera technology. Figure 3 shows a schematic of the sensor. Continuous wave light from a high-power fiber laser (IPG Phontonics GLR-50) was directed into an acousto-optic modulator (AOM), which generated 20-100 ns pulses at a repetition rate of 40 kHz. Using a half-wave plate (HWP) and polarizing beam splitter, 80% of the light (~1 W peak) was directed into 2 km of graded-index multimode fiber (Corning OM2). The fiber has a 50 μm core, a numerical aperture of 0.2, and supports about 870 spatial modes at 532 nm. The remainder of the light was sent to a reference arm. The reference arm served two functions: first, it provided a mechanism with which to select for light backscattered from a specific region within the fiber as indicated in the inset in the upper right corner of Fig. 3, and, second, it mitigated the effects of camera dark noise despite the relatively low backscattered light levels.

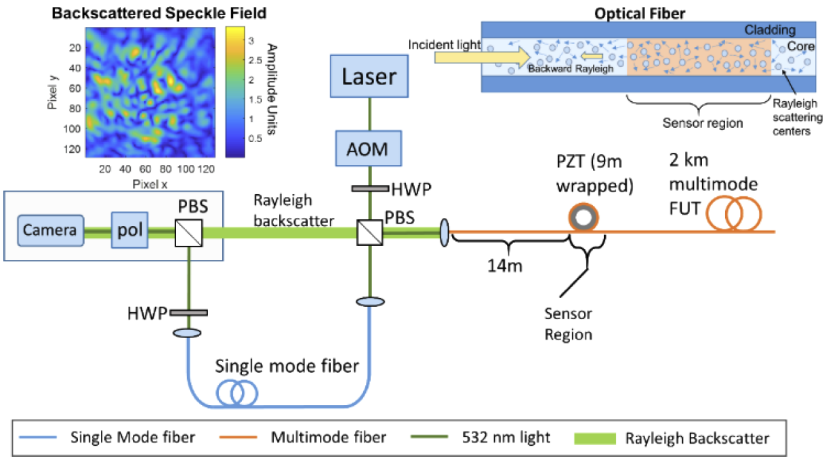

Fig. 3. Schematic of multimode fiber strain sensor. The inset in the upper right hand corner shows a cartoon of the Rayleigh scattering within the multimode fiber. The inset in the upper left hand corner shows the recorded backscattered speckle field from the multimode fiber.

Rayleigh scattered light from the multimode fiber was directed to a high speed camera (Vision Research Phantom v2512) which collected 128×128 pixel images at a frame rate of 40 kHz and an integration time of 276 ns. The inset in the upper left corner of Fig. 3 shows a representative backscattered speckle field measured with the camera. Light from the reference arm was directed into the camera at a small angle with respect to the Rayleigh backscatter. Off-axis holography was used to extract the time varying amplitude of the backscattered speckle field as described previously [26,29]. Briefly, a 2-dimensional Fourier transform of the raw image allowed us to identify the spatial frequencies associated with the speckle pattern. A Hann window filter

Optics EXPRESS

was applied around those spatial frequencies in the Fourier domain and an inverse Fourier transform was used to recover the amplitude and phase of the speckle field. In this work the phase information was discarded. For most of the data shown in this paper, 10,000 frames were collected over 250 ms. The speckle amplitude recovery process was completed for each frame collected with the camera, providing a time-dependent amplitude at each pixel.

To test the sensor, 9 m of multimode fiber was wrapped on a piezoelectric (PZT) cylinder. The PZT was driven with a voltage to induce strain in the fiber. The PZT was positioned 14 m from the end of the fiber. The sensor spatial resolution was dictated by the pulsewidth of the input light as $dz \cong \frac{Tc}{2n}$. For a 100 ns pulse, the sensor resolution is 10 m while a 20 ns pulse provided a 2 m sensor. For most of the experiments reported here, the sensor region was positioned to overlap with the position of the PZT by choosing an appropriate length of SMF in the reference arm. In our current implementation, changing the sensor position required us to change the length of SMF in the reference arm. However, the sensor position could, in general, be reconfigured electronically if the reference arm was pulsed separately from the probe arm (e.g. by using a second AOM). This approach would result in a path mismatch between the Rayleigh backscattered light and the reference arm. Fortunately, since our approach relies on the amplitude of the backscattered speckle field, rather than the phase with respect to the reference arm, the only requirement is that the laser be sufficiently coherent for the reference arm to interfere with the backscattered light. This is a benefit of the current approach in comparison to our prior work which was extremely sensitive to any path mismatch [26].

4.2. Testing sensor performance

We first tested the sensor under a linearly increasing strain, analogous to the simulated test shown in Fig. 2. Figure 4(a) shows the amplitude of one pixel as a function of time along with the assigned pixel flags when a linearly increasing strain is applied to the fiber. Clearly, the flags are correctly assigned in the presence of experimental noise. Figure 4(b) shows that the algorithm correctly recovers the linearly increasing strain. To test the algorithm further, a 50 Hz sinusoidal waveform and then a 50 Hz saw tooth waveform was applied to the PZT and the results are shown in Fig. 4(c) and Fig. 4(d), respectively. The results show that the algorithm is able to distinguish between a saw tooth and sinusoidal strain oscillations, indicating the large amount of information contained within the speckle amplitude fluctuations.

4.3. Measuring sensor responsivity

In order to experimentally measure the sensor responsivity, we first measured the strain imparted by the PZT on the fiber. This was achieved by constructing a separate Mach-Zehnder interferometer in which the fiber wrapped PZT composed one arm of the interferometer. A sinusoidal signal was applied to the PZT and the phase was recorded using the technique described in [29] and [26], providing a PZT strain response of 114.7 nε/V.

The speckle tracking sensor was then setup as shown in Fig. 3 with the PZT positioned 14 m down the fiber. For this measurement, in order to ensure that constant strain was experienced throughout the sensor region, the pulsewidth was reduced to 20 ns (sensor length of 2 m) so that the sensor region fit well inside the 9 m of fiber wrapped around the PZT. The PZT was driven with a 1 kHz sine wave at a voltage of 100 mVpp. The signal in amplitude units (a.u.) was measured with the speckle tracking algorithm and the PZT strain response given above was used to determine the amount of strain imparted to the fiber. The responsivity was scaled by the 2 m sensor length to yield:

$$R_{meas} = 5.63 \times 10^{-3} \text{au/n}\varepsilon\text{/m}.$$

The agreement with the predicted responsivity based on the simulated data is quite good considering the relatively simplified 1-dimensional model which ignored effects such as mode mixing. Throughout this work, the experimentally measured responsivity was used to convert

Optics EXPRESS

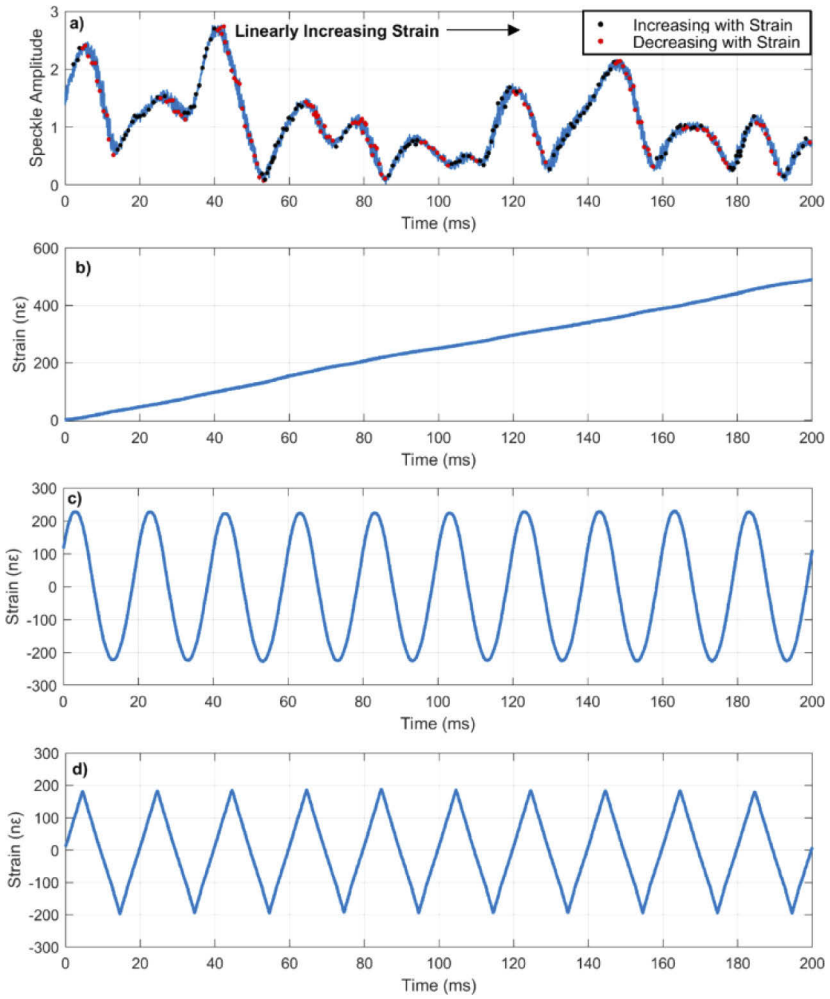

Fig. 4. a) Amplitude of a single pixel as a linearly increasing strain is applied to the fiber. The black dots indicate that the amplitude of this pixel increases with increasing strain during a given time period while the red dots indicate that the amplitude decreases with increasing strain. b) The recovered strain extracted from the amplitude fluctuations of the backscattered speckle pattern when a linear strain was applied to the fiber. c) The recovered strain when a 50 Hz sinusoidal strain was applied to the fiber by the PZT. d) The recovered strain when a 50 Hz saw tooth strain was applied to the fiber by the PZT.

Optics EXPRESS

the measured amplitude units extracted by the speckle tracking algorithm to units of strain. Note that by converting the measured speckle pattern to normalized amplitude units we can use this sensor responsivity for sensors at different positions in the fiber or for different fibers altogether.

4.4. Further characterizing sensor performance

To evaluate the limits over which the sensor provides quantitative strain response, we conducted a linearity test. A 1 kHz sinusoidal waveform was applied to the PZT at a range of voltages from 2 mVpp to 500 mVpp. The measured strain recorded at each voltage is plotted in Fig. 5(a). The data show there is a linear response for strains up to 15 nε. It is clear from the plot that for larger strains, the response no longer behaves linearly and therefore 15 nε represents the experimentally determined maximum detectable strain at 1 kHz.

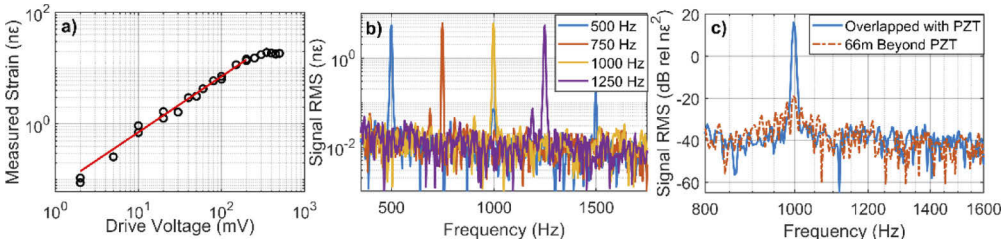

Fig. 5. a) Measured response of the sensor as a PZT was driven with a 1 kHz sine wave with voltages from 2 mVpp to 500 mVpp. The response is linear for measured strains up to 15 nε, but saturates above this value due to the effective slew rate limit of the sensor. b) Frequency response of the sensor as a PZT was driven with a 100 mVpp sine wave with frequencies of 500 Hz, 750 Hz, 1000 Hz, and 1250 Hz. c) Response to a PZT driven with a 1 kHz, 180 mVpp sine wave when the sensor region is overlapped with PZT (solid blue line) and when the sensor region is positioned 66 m beyond the PZT position (orange dashed line). The response to the PZT was suppressed by 38 dB in the latter measurement.

In conventional interferometric fiber strain sensors, measurements of large strains are limited by the slew rate of the interferometer, which occurs when the signal induces a π phase change between samples. The sensor described in this work does not measure the phase, but is still limited by an analogous slew rate, which occurs when the signal is strong enough that the speckle pattern begins to decorrelate between consecutive frames. We can describe this limit quantitatively by requiring that the change in the speckle pattern between frames remain below the threshold used to update the sign flags for this work: dA_{thresh} = 0.15a.u. This value of dA_{thresh} was the optimal value for recovering the strain based on the signal-to-noise level and higher-order distortion. As in a traditional interferometer, the maximum detectable strain is a function of signal amplitude and frequency. Given a dA_{thresh} of 0.15 amplitude units and a signal frequency of 1 kHz, we expect a maximum detectable strain of 17 nε, in excellent agreement with the experimental measurements.

In order to test the frequency response of the sensor, we measured strains while driving the PZT with a 100 mVpp sinusoidal waveform with frequencies from 500 Hz to 1250 Hz. As shown in Fig. 5(b), the sensor response is flat across the measured frequency band.

To confirm that the sensor only responds to vibrations within the sensor region, the sensor region was positioned 66 m past the PZT. The PZT was driven with a 180 mVpp 1 kHz sine wave and the response was recorded. The power spectral density of the response is shown as an orange dashed line in Fig. 5(c). Also shown in Fig. 5(c) as the solid blue line is the response when the sensor region was overlapped with the PZT. The signal was suppressed by about 38 dB when the sensor region was not overlapped with the vibration.

Optics EXPRESS

The strain noise of the sensor was measured with a 1 Hz sawtooth waveform applied to the PZT. The signal was applied to the PZT to ensure that the speckle tracking algorithm was operating throughout the measurement and maintaining the correct sign flags. Figure 6(a) shows the amplitude spectral density of the noise of the multimode fiber sensor. The sharp peak at 3.8 kHz is aliased frequency noise from the laser. A minimum detectable strain of 2.9 p$\varepsilon/\sqrt{\text{Hz}}$ is achieved. Using the maximum detectable strain at 1 kHz determined from the test shown in Fig. 6(a), the dynamic range at 1 kHz is 74 dB.

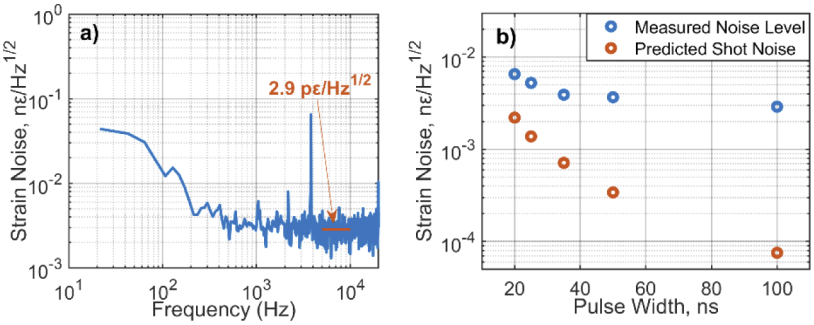

Fig. 6. a) Power spectral density of the strain noise measured for the multimode fiber sensor. The peak at 3.8 kHz is due to laser frequency noise. b) The strain noise was measured for five pulsewidths between 20 ns and 100 ns. Also shown on the plot is the predicted shot noise of the sensor at each pulsewidth. The divergence from the shot-noise limit for longer pulse widths indicates that the sensor was laser phase noise limited in that regime.

To determine the limiting factor to the noise of the sensor, the strain noise was measured using five pulsewidths from 20 ns to 100 ns as shown in Fig. 6(b). We expect to achieve lower strain noise for longer pulses due to two effects. First, since the peak power of our laser was fixed, longer pulses enable us to collect higher light levels and achieve lower shot noise. Second, the responsivity factor scales with the length of the sensor because a fixed strain introduces a larger displacement between scattering centers further away from each other. An analytic expression of the strain noise for the sensor was derived to have a power spectral density in units of ε^2/Hz of

$$S_\varepsilon(f) = \frac{1}{N_{pix} f_s T m \eta P_{pix}} \frac{2h\nu}{} \left(\frac{1}{R_{meas} L}\right)^2 \tag{2}$$

where h is Plank's Constant, ν is the optical frequency, N_{pix} is the number of pixels used in each frame, f_s is the camera frame rate (also the pulse repetition frequency), T is the pulsewidth, m is the mixing efficiency, η is the quantum efficiency of the camera, P_{pix} is the average power on each pixel, R_{meas} is the measured sensor responsivity, and L is the sensor length.

The experimentally measured strain noise is shown as a function of pulsewidth along with the theoretical shot noise limit in Fig. 6(b). Experimentally, we found that the strain noise decreased initially with pulse duration as expected but was relatively constant for pulse widths from 35 ns to 100 ns. This indicated that laser phase noise was a limiting factor in this regime. Note that although this approach is not sensitive to the impact of laser phase noise on the relative phase between the reference arm and the pulse entering the fiber, it is sensitive to the phase noise during the pulsewidth which will impact the repeatability of the amplitude of the backscattered speckle field. At 20 ns the measured noise level is within a factor of 3 of the predicted shot noise limit, while laser phase noise limited the 100 ns pulse measurement to 32 dB above the shot noise limit. We therefore expect that lower noise could be achieved by using a laser with lower-phase noise (in the case of pulses >35 ns) or higher peak power (in the case of pulses <35 ns).

Optics EXPRESS

5. Conclusion

In summary, we presented a multimode fiber based dynamic strain sensor that uses the evolution of the backscattered speckle pattern to extract a linear strain response. Multimode fiber based strain sensors have several advantages compared with single mode fiber sensors including a higher power threshold for nonlinear effects and complete immunity from signal fading. In addition, the diversity of spatial modes in a multimode fiber provides sufficient information to perform quantitative strain measurements using only the amplitude of the backscattered speckle pattern. Extracting strain directly from the amplitude of the speckle pattern has several advantages in terms of sensor reconfigurability and reduced sensitivity to laser phase noise. The sensor exhibits a high degree of linearity, a flat frequency response, and nearly 40 dB of common mode rejection at 1 kHz. The sensor has a minimum detectable strain of 2.9 p$\varepsilon/\sqrt{\text{Hz}}$, a bandwidth of 20 kHz, and a dynamic range of 74 dB at 1 kHz. In this work 532 nm light was used to take advantage of existing camera technology, but recent advanced in high-speed InGaAs cameras could enable the same approach at telecom wavelengths.

Appendix

Here we give the details of the algorithm developed to extract quantitative strain information from the recorded speckle pattern scattered out of a multimode fiber.

1. The amplitude of each recorded pixel is normalized to the average amplitude of the entire speckle pattern recorded for that frame. This results in a standard scale for the amplitude of each data set, which we refer to as being in amplitude units (a.u.). The normalization removes relative intensity noise from the data and enables us to calculate a conversion factor from a.u. to strain that is independent of the backscattered light level and detector responsivity.

2. A low-pass filter with a pass band of 5 kHz and stop band of 10 kHz is applied to the data to remove spurious high frequency intensity changes that can degrade performance. This also ensures that the changes in the speckle pattern that set the sign of the speckle grains are due to strain in the fiber rather than simply noise in the measurement.

3. The numerical derivative of the amplitude evolution is calculated for each pixel:

$$A'_m(n) = A_m(n+1) - A_m(n) \tag{3}$$

   where A is the intensity, n is the frame number, and m is the pixel number.

4. The value of the derivative is accumulated from $n_i = n_{start}$ to a frame N:

$$\Delta A_m = \sum_{n=n_{start}}^{N} A'_m(n) \tag{4}$$

   The value of N is such that the median of $|\Delta A_m|$ reaches a user-defined threshold dA_{thresh}. Initially, pixels are given pixels flags $f_m(n)$ based on the sign of ΔA_m.

5. The strain direction d is determined by the previous pixel flags andΔA_m:

$$d = \text{sgn}(\langle f_m(n_{start} - 1)\Delta A_m \rangle) \tag{5}$$

6. New pixel flags are assigned based on the strain direction and the sign of ΔA_m:

$$f_m\left(n_{start} \rightarrow \frac{n_{start} + N}{2}\right) = \text{sgn}(\Delta A_m) \times d \tag{6}$$

Optics EXPRESS

7. The new initial frame is assigned: $n_i = \frac{n_{start}+N}{2} + 1$

8. Steps 4-7 are repeated until N reaches the end of the recorded frames.

9. The change in strain $d\varepsilon(n)$ is determined by averaging the change in intensity with the pixel flags over all pixels:

$$d\varepsilon(n) = \frac{1}{M}\sum_m f_m(n)A'_m(n) \tag{7}$$

where M is the total number of pixels. The raw unfiltered derivative is used in Eq. (7) to maximize the sensor bandwidth.

10. The strain $\varepsilon(n)$ as a function of time (frame) is:

$$\varepsilon(n) = \sum_{n=1}^{n} d\varepsilon(n) \tag{8}$$

The result is a quantitative measurement of the strain in the fiber as a function of time. While the algorithm was implemented in post processing in this work, the algorithm itself is entirely forward processing and so, with some latency, the strain could be recovered in real time.

Funding

U.S. Naval Research Laboratory (6.2 Base Program).

References

1. D. J. Richardson, J. M. Fini, and L. E. Nelson, "Space-division multiplexing in optical fibres," Nat. Photonics **7**(5), 354–362 (2013).
2. J. M. Kahn and D. A. B. Miller, "Communications expands its space," Nat. Photonics **11**(1), 5–8 (2017).
3. M. Plöschner, T. Tyc, and T. Čižmár, "Seeing through chaos in multimode fibres," Nat. Photonics **9**(8), 529–535 (2015).
4. B. Redding and H. Cao, "Using a multimode fiber as a high-resolution, low-loss spectrometer," Opt. Lett. **37**(16), 3384–3386 (2012).
5. L. G. Wright, D. N. Christodoulides, and F. W. Wise, "Controllable spatiotemporal nonlinear effects in multimode fibres," Nat. Photonics **9**(5), 306–310 (2015).
6. A. Masoudi and T. P. Newson, "Contributed review: Distributed optical fibre dynamic strain sensing," Rev. Sci. Instrum. **87**(1), 011501 (2016).
7. J. M. Lopez-Higuera, L. Rodriguez Cobo, A. Quintela Incera, and A. Cobo, "Fiber optic sensors in structural health monitoring," J. Lightwave Technol. **29**(4), 587–608 (2011).
8. J. C. Juarez and H. F. Taylor, "Distributed fiber optic intrusion sensor system," J. Lightwave Technol. **23**(6), 2081–2087 (2005).
9. G. A. Cranch, P. J. Nash, and C. K. Kirkendall, "Large-scale remotely interrogated arrays of fiber-optic interferometric sensors for underwater acoustic applications," IEEE Sens. J. **3**(1), 19–30 (2003).
10. Z. Tian, S. S.-H. Yam, J. Barnes, W. Bock, P. Greig, J. M. Fraser, H.-P. Loock, and R. D. Oleschuk, "Refractive index sensing with Mach-Zehnder interferometer based on concatenating two single-mode fiber tapers," IEEE Photonics Technol. Lett. **20**(8), 626–628 (2008).
11. L. Li, L. Xia, Z. Xie, and D. Liu, "All-fiber Mach-Zehnder interferometers for sensing applications," Opt. Express **20**(10), 11109 (2012).
12. Y. Zhang, L. Xia, C. Cao, Z. Sun, Y. Li, and X. Zhang, "A hybrid single-end-access MZI and Φ-OTDR vibration sensing system with high frequency response," Opt. Commun. **382**, 176–181 (2017).
13. F. Zhu, Y. Zhang, L. Xia, X. Wu, and X. Zhang, "Improved Φ-OTDR sensing system for high-precision dynamic strain measurement based on ultra-weak fiber bragg grating array," J. Lightwave Technol. **33**(23), 4775–4780 (2015).
14. R. Juskaitis, A. M. Mamedov, V. T. Potapov, and S. V. Shatalin, "Interferometry with Rayleigh backscattering in a single-mode optical fiber," Opt. Lett. **19**(3), 225–227 (1994).
15. Y. Muanenda, C. J. Oton, S. Faralli, and F. Di Pasquale, "A cost-effective distributed acoustic sensor using a commercial off-the-shelf DFB laser and direct detection phase-OTDR," IEEE Photonics J. **8**(1), 1–10 (2016).
16. A. Masoudi, M. Belal, and T. P. Newson, "A distributed optical fibre dynamic strain sensor based on phase-OTDR," Meas. Sci. Technol. **24**(8), 085204 (2013).

Optics EXPRESS

17. G. J. Tu, X. P. Zhang, Y. X. Zhang, F. Zhu, L. Xia, and B. Nakarmi, "The development of an Φ-OTDR system for quantitative vibration measurement," IEEE Photonics Technol. Lett. **27**(12), 1349–1352 (2015).
18. M. Nakazawa, "Rayleigh backscattering theory for single-mode optical fibers," J. Opt. Soc. Am. **73**(9), 1175–1180 (1983).
19. P. Healey, "Fading in heterodyne OTDR," Electron. Lett. **20**(1), 30–32 (1984).
20. A. H. Hartog, L. B. Liokumovich, N. A. Ushakov, O. I. Kotov, T. Dean, T. Cuny, A. Constantinou, and F. V. Englich, "The use of multi-frequency acquisition to significantly improve the quality of fibre-optic-distributed vibration sensing," Geophys. Prospect. **66**(S1), 192–202 (2018).
21. M. Zabihi, Y. Chen, T. Zhou, J. Liu, Y. Shan, Z. Meng, F. Wang, Y. Zhang, and M. Chen, "Continuous Fading Suppression Method for Φ -OTDR Systems Using Optimum Tracking Over Multiple Probe Frequencies," J. Lightwave Technol. **37**(14), 3602–3610 (2019).
22. K. Pan, C. Uang, F. Cheng, and F. T. S. Yu, "Multimode fiber sensing by using mean-absolute speckle-intensity variation," Appl. Opt. **33**(10), 2095–2098 (1994).
23. Z. Zhang and F. Ansari, "Fiber-optic laser speckle-intensity crack sensor for embedment in concrete," Sens. Actuators, A **126**(1), 107–111 (2006).
24. L. Rodriguez-Cobo, M. Lomer, A. Cobo, and J.-M. Lopez-Higuera, "Optical fiber strain sensor with extended dynamic range based on specklegrams," Sens. Actuators, A **203**, 341–345 (2013).
25. E. Fujiwara, L. E. da Silva, T. H. R. Marques, and C. M. B. Cordeiro, "Polymer optical fiber specklegram strain sensor with extended dynamic range," Opt. Eng. **57**(11), 1 (2018).
26. M. J. Murray, A. Davis, and B. Redding, "Multimode fiber Φ-OTDR with holographic demodulation," Opt. Express **26**(18), 23019 (2018).
27. K. Okamoto, *Fundamentals of Optical Waveguides*, II (Elsevier, 2006).
28. R. Posey, G. A. Johnson, and S. T. Vohra, "Strain sensing based on coherent Rayleigh scattering in optical fibre," Electron. Lett. **36**(20), 1688–1689 (2000).
29. B. Redding, A. Davis, C. Kirkendall, and A. Dandridge, "Measuring vibrational motion in the presence of speckle using off-axis holography," Appl. Opt. **55**(6), 1406–1411 (2016).